Probing Single-Molecule Fluorescence Spectral Modulation within Individual Hotspots with Subdiffraction-Limit Image Resolution

ARTICLE *in* ANALYTICAL CHEMISTRY · MARCH 2013

Impact Factor: 5.64 · DOI: 10.1021/ac400240v · Source: PubMed

7 AUTHORS, INCLUDING:

Chang Liu
University of British Columbia - Vancouver
15 PUBLICATIONS **191** CITATIONS
SEE PROFILE

Lehui Xiao
Hu Nan Normal University
22 PUBLICATIONS **297** CITATIONS
SEE PROFILE

analytical chemistry

Article

pubs.acs.org/ac

Probing Single-Molecule Fluorescence Spectral Modulation within Individual Hotspots with Subdiffraction-Limit Image Resolution

Lin Wei,[†,‡,∥] Chang Liu,[§,∥] Bo Chen,[‡] Peng Zhou,[‡] Hongchang Li,[‡] Lehui Xiao,*[,‡] and Edward S. Yeung*[,§]

[†]College of Chemistry and Chemical Engineering, College of Biology, State Key Laboratory of Chemo/Biosensing and Chemometrics, Hunan University, Changsha, 410082, P. R. China

[‡]Key Laboratory of Chemical Biology & Traditional Chinese Medicine Research, Ministry of Education, College of Chemistry and Chemical Engineering, Hunan Normal University, Changsha, Hunan, 410081, P. R. China

[§]Ames Laboratory-U.S. Department of Energy and Department of Chemistry, Iowa State University, Ames, Iowa, 50011, United States

Supporting Information

ABSTRACT: The enhancement of the electromagnetic field on the rough metallic nanostructure has been extensively applied to obtain chemical or biological information about molecules with high sensitivity and has received much attention due to its potential applications in new types of devices based on nanoelectronics and nanophotonics. The typical size of the field enhancement area, the so-called hotspot, is approximately 1 order of magnitude smaller than the optical diffraction limit. In the present study, an optical super-resolution microscopic and spectroscopic approach is introduced to explore single-molecule fluorescence within a hotspot where nonhomogeneous spectral modulation is resolved beyond the optical diffraction limit for the first time. Distinct Stokes shifts from individual dyes were directly observed within single hotspots, which were found to be independent of the local electromagnetic field strength. The method reported here provides a robust tool to probe the optical properties of nanoresonantors with high temporal and spatial resolution.

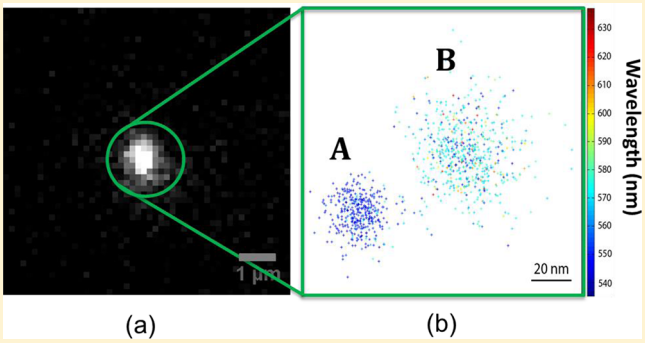

When the light illuminates a metallic nanostructure, it may be concentrated on the nanometer scale to produce a significantly enhanced electromagnetic field that enables the detection of weak optical signals. This phenomenon, called surface enhancement, has been extensively adopted for the studies of surface enhanced Raman scattering (SERS) and surface enhanced fluorescence.[1−3] Recent experimental and theoretical works on nano-optics have demonstrated that the surface enhancement effect is associated with the strong electromagnetic response of the metallic nanostructure (hotspot), particularly when localized surface plasmon resonance is excited.[4,5] Furthermore, quantitative experimental studies on the fluorescence intensity have illustrated that the quantum yield of the emitter varies as a function of the distance between the nanoantenna,[6] which is also confirmed by fluorescence lifetime mapping results.[7] These findings show that the localized electromagnetic field distribution around the nanoantenna together with the fluorescence quantum yield modulation effect determine the fluorescence enhancement functionality. Despite these remarkable achievements in either theoretical or experimental investigations, another important parameter, the spatially dependent fluorescence spectral modulation effect within the nanoantenna, is rarely discussed so far due to challenges such as detection sensitivity, photostability, and especially position control. However, understanding the fluorescence spectral modulation effect of a multilevel energy system (such as a fluorescent molecule) within a hotspot is especially important because the resonant transitions inside a nanoantenna can be enhanced while the nonresonant transitions are suppressed. Therefore, the net fluorescence spectral profile of the emitter will be changed as a result of a modification of the energy levels of the emitter.[8]

To overcome those challenges in this nanoscale system, several techniques have been developed with high spatial resolution. Imura et al. applied scanning near-field optical microscopy (SNOM) to interrogate the electromagnetic field around dispersed metallic rods,[9] and nanoantennas have been imaged with scattering type SNOM in a recent study.[10] Nevertheless, the SNOM probe itself might affect the resonance condition and modify the optical properties of the emitter. In this regard, a noninvasive optical imaging method

Received: January 23, 2013
Accepted: March 1, 2013
Published: March 1, 2013

   dx.doi.org/10.1021/ac400240v | *Anal. Chem.* 2013, 85, 3789−3793

with nanometer-sized resolution and single molecule sensitivity is preferred. In this work, we overcame the above challenges through an optical super-resolution microscopic and spectroscopic approach. With this method, we probed the spatially dependent single molecule fluorescence spectral modulation effect within individual hotspots with nanometer resolution for the first time.

EXPERIMENTAL SECTION

Chemicals and Materials. Anhydrous ethylene glycol (EG), platinum chloride ($PtCl_2$), silver nitrate ($AgNO_3$), poly(vinyl pyrrolidone) (PVP, MW ≈ 55 000), cysteamine, Rhodamine B, and bovine serum albumin (BSA) were purchased from Sigma Aldrich (St. Louis, MO), and silver nanosphere (~30 nm) was purchased from Nanopartz Inc. (Loveland, CO).

Synthesis of Silver Nanowire. Silver nanowires were synthesized according to a reported method[11] by reducing silver nitrate with EG in the presence of Pt and PVP. Briefly, 0.5 mL of $PtCl_2$ solution (1.5×10^{-4} M, in EG) was added into 5 mL of EG and heated at 160 °C in a round-bottom flask. After 4 min, 2.5 mL of $AgNO_3$ solution (0.12 M in EG) and 5 mL of PVP solution (0.36 M, in EG) were simultaneously added to the hot solution over a period of 6 min. The reaction mixture was heated to 160 °C until all $AgNO_3$ had been reduced. The silver nanowire was then purified by centrifugation and washed three times with DI water. The scattering image from a silver nanowire is shown in Figure S1 in the Supporting Information.

Hotspot Fabrication. The synthesis of hotspots along the nanowire was carried on in a flow channel with a width around 5 mm. First, the cleaned glass slide was modified with (3-aminopropyl)triethoxysilane (APTES). Silver nanowires were then introduced into the flow channel and fixed on the wall of the glass slide through electrostatic interaction. A dilute BSA solution (0.01 mg/mL) was subsequently flowed into the channel to block the excessive binding sites on the cover glass surface. In order to specifically conjugate silver nanospheres to the side wall of the silver nanowire, a 50 mM cysteamine solution was introduced to the channel to partially modify the silver nanowire with amine groups. Excessive reagents were then flushed away by washing the channel with DI water. Finally, a silver nanosphere solution (around 0.1 nM) was introduced into the channel, coupling with the fixed silver nanowire through electrostatic interaction to form artificial hotspots. Additional nanospheres were washed away by DI water.

Setup and Image Analysis. A home-built prism-type total internal reflection florescence (TIRF) microscope with a 100× Plan Apo/1.40 oil-immersion objective was used for the single molecule fluorescence imaging. A 532 nm diode laser was adopted to excite the fluorescence from Rhodamine B. The optical signals were recorded with an EMCCD (Evolve, Photometrics) after being filtered by a 532 nm long pass filter (BLP01-532R-25, Semrock). In the single molecule spectral imaging experiment, a transmission grating beam splitter (70 grooves/mm) was placed in front of the camera to simultaneously record the molecular location (zeroth-order image) and the fluorescence spectrum (wavelength-resolved first-order image), Figure S2 in the Supporting Information. To probe the size and spectral modulation effect of the hotspot, the Rhodamine dye solution (around 0.1 nM) was slowly introduced into the flow channel. The random adsorption process enables the visualization of the hotspot on the nanowire by superlocalization imaging.[12] The exposure time of the camera was set to be 10 ms. The collected images were analyzed by MATLAB or ImageJ (http://rsbweb.nih.gov/ij/). For super-resolution imaging, the fluorescent spots were fitted to a two-dimensional Gaussian function[12]

$$F(x, y, z_o, A, x_o, y_o, s_x, s_y) = z_o + A \exp\left[-\frac{1}{2}\left[\left(\frac{(x - x_o)}{s_x}\right)^2 + \left(\frac{(y - y_o)}{s_y}\right)^2\right]\right]$$

where z_o is a constant term from the background noise, A is the amplitude, x_o and y_o are the coordinates of the center, and s_x and s_y are standard deviations of the distribution in the x and y direction. As discussed by Thompson et al.,[13] the localization precision (σ) of this curve-fitting strategy is sensitive to the number of collected photons (N), the pixel size of the imaging detector (a), the radius of the point-spread function (s), and the background noise of the detector (b), which can be quantified as

$$\sigma = \sqrt{\left(\frac{s^2}{N} + \frac{a^2}{12N} + \frac{8\pi s^4 b^2}{a^2 N^2}\right)}$$

In this study, with a pixel size of 160 nm, a radius of the point-spread function s = 320 nm, b = 12, and $N \approx 43\,247$ (from a "weak" fluorescent spot with intensity less than 10% of the maximum value), the localization error σ is as small as 1.8 nm.

RESULTS AND DISCUSSION

We first fabricated the nanoantenna for fluorescence enhancement based on the silver nanowire-nanoparticle system that has been adopted as a typical hotspot generation platform whereby studies of chemical sensing and imaging based on the field enhancement effect have been extensively reported.[14] Silver nanowires were introduced into a flow channel and fixed on the cover glass. BSA was used to block the excessive adsorption sites on the cover glass surface. Silver nanosphere (with a size around 30 nm) solution was then introduced and vigorous thermal diffusion due to heating enables the random coupling of silver nanospheres close to the silver nanowire via electrostatic interactions, which effectively forms the desired hotspots along the nanowire for fluorescence enhancement. In the control experiment (without silver nanosphere), we found that it was very hard to observe any fluorescent hotspots along the bare silver nanowire.

Among the current fluorescence-based super-resolution imaging techniques, such as stochastic optical reconstruction microscopy (STORM)[15] and photoactivated localization microscopy (PALM),[16] photoswitchable dyes are typically required that can be stochastically modulated between the on and off states. Therefore, those spatially separated fluorophores can be independently localized by a two-dimensional Gaussian fit with nanometer accuracy.[12] In the present study, the basic idea to achieve two-dimensional super-resolution in a dynamic solution is to take advantage of the reversible adsorption/desorption events of individual dye molecules (Rhodamine B) in a laminar flow.[17−19] Through controlling the dye concentration, the condition that essentially only one molecule at a time is adsorbed onto the individual hotspot and emits can be assured. After the dye is flushed or diffused away, the

dx.doi.org/10.1021/ac400240v | Anal. Chem. 2013, 85, 3789−3793

fluorescent signal disappears and the hotspot is then ready for the next adsorption event.

As a proof of concept experiment, we tested the super-resolution imaging capability of this strategy in the silver nanowire-nanoparticle system. From the conventional fluorescence image in Figure 1a, we note that only a few bright

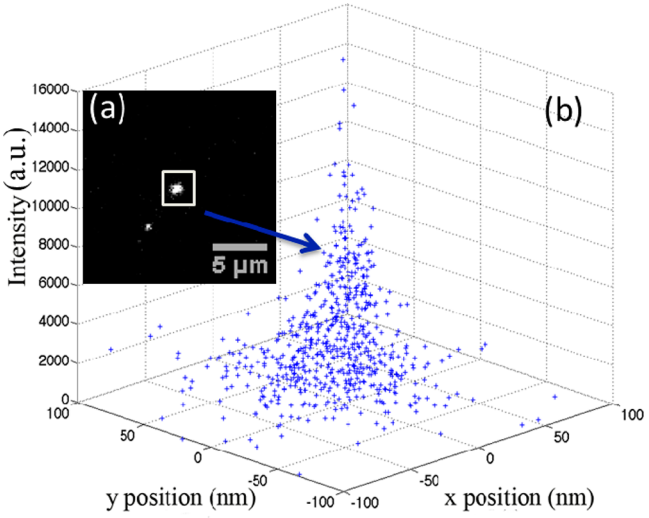

Figure 1. (a) Conventional wide-field fluorescence image of hotspots with an exposure time of 10 ms. (b) Superlocalization profile of the highlighted hotspot.

spots can be observed in the hotspot areas despite the relatively high concentration of the dye (0.1 nM). This is because the interfering signals from randomly adsorbed dyes elsewhere are typically several times weaker than that within a hotspot. By carefully setting the intensity threshold of the light source, those interfering signals from the solution or on the cover glass surface can be effectively excluded, which is the key step for the subsequent spatial localization.

Figure 1b demonstrates a typical superlocalized fluorescence enhancement profile from a hotspot on a silver nanowire. The maximum fluorescence enhancement from the hotspot was observed in the center of the profile and decayed rapidly along the axial directions. Because of the strong field confinement effect from the hotspot, the full-width at half-maximum (fwhm) of this profile is as small as 30 nm, in line with the observations as reported elsewhere.[19−21]

One of the remarkable advantages from this super-resolution strategy is that we can readily resolve spatially separated individual hotspots beyond the optical diffraction limit, which might represent distinct optical modulation properties. A typical example is demonstrated in Figure 2. In the conventional fluorescence image (Figure 2a), the fluorescent signals arising from the dyes adsorbed in closely separated hotspots (A or B) only generate an unresolvable single bright spot with approximately the diffraction limit size. Therefore, the photophysical information derived from a conventional optical imaging method cannot reflect the true photophysical information in space. With the noninvasive super-resolution approach, the exact positions of the adsorbed dyes can be determined and discriminated, and thus the photophysical information from these two conjugated hotspots can be clearly differentiated. As demonstrated in Figure 2b, the center-to-center distance between hotspots A and B is only around 60

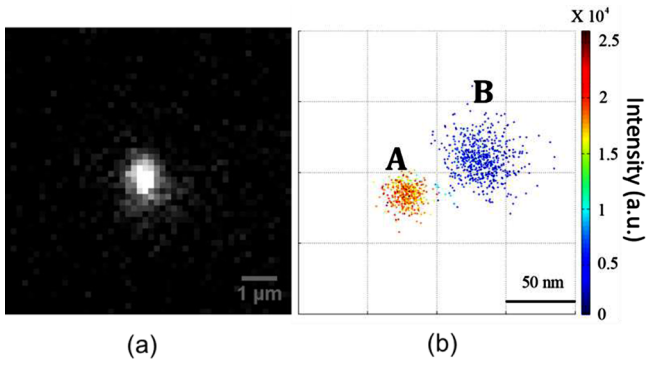

Figure 2. Super-resolution imaging of single molecules in a conjugated hotspot region. (a) Conventional wide-field fluorescence image of Rhodamine B adsorbed in the observation area (with an exposure time of 10 ms). (b) Super-resolution imaging in the same area. Two hotspots with about 60 nm separation can be completely differentiated. The intensities of the fluorescent signals originating from the individual dyes are encoded with different colors.

nm, while the enhancement effect from hotspot A is significantly stronger than that from hotspot B (~7×).

Ringler's experimental results verify that the fluorescence spectra of Cy3 molecules within nanoparticle dimers can be synchronized by tuning the resonance frequency of the nanoantenna (for example, the gap distance).[8] Nevertheless, their measurements are ensemble-averaged results that mask the spatially dependent wavelength modulation effect within the hotspot. From this point of view, it is important to understand in detail the fluorescence spectral modulation effect with nanometer resolution and at the single molecule level.

With this regard, we further derived the single molecule fluorescence spectral information inside the hotspot. To realize this goal, a transmission grating beam splitter (70 grooves/mm) was placed in front of the CCD camera. This allows the simultaneous imaging of the undeviated zeroth-order image and the wavelength-resolved first-order image.[22] As mentioned above, through controlling the dye concentration, the adsorption rate can be manipulated to ensure that only one dye at a time emits fluorescence in the observation region. The random blinking trajectory directly proves that the fluorescent signals did not originate from multiple dyes residing closely in space (Figure S3 in the Supporting Information). By correlating the temporal information of the superlocalized hotspots, the single molecule fluorescence spectra at different locations can be readily distinguished.

Figure 3 shows the spatially encoded single molecule fluorescence spectral information from hotspots A and B. For the molecules resided inside hotspot A, two types of modulated fluorescence spectra were clearly resolved. The majority of the dyes have an emission maximum of 550 ± 5 nm. Only a small fraction of the molecules (~15%) exhibit a fluorescence maximum at 570 ± 5 nm, with almost no molecules with emission located longer than 600 nm. Within hotspot B, which is only about 60 nm away from hotspot A, the single molecule fluorescence spectral modulation effect is remarkably different. Three types of emission were resolved as indicated in the histogram of fluorescence spectra, Figure 4a,b. The largest population (~75%) was red-shifted to 570 ± 5 nm (the minor fraction in hotspot A). In only about 20% of the cases, the molecules showed an emission maximum at 550 ± 5 nm.

dx.doi.org/10.1021/ac400240v | Anal. Chem. 2013, 85, 3789−3793

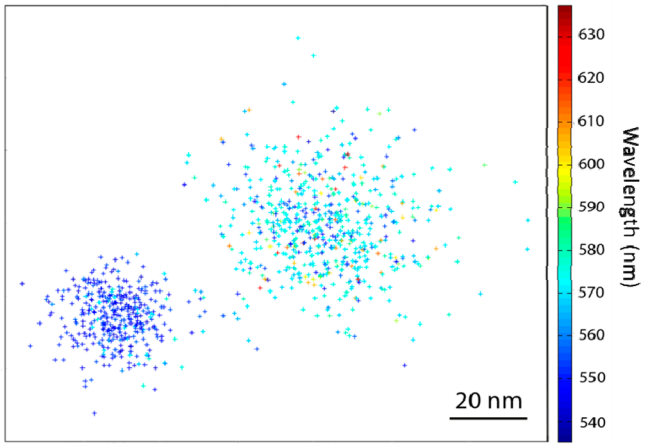

Figure 3. Fluorescence spectral distribution of individual Rhodamine B molecules in the hotspots A and B in Figure 2.

Occasionally, we could also observe some dyes with an emission maximum longer than 600 nm.

These interesting observations indicate that the fluorescence spectral modulation effect inside the hotspot is not a spatially homogeneous process at the single-molecule level, which is hard to be explained purely based on the generalized electromagnetic theory (i.e., Mie theory).[8] It is worthwhile to note that the above spatially encoded information is very difficult to be accessed by utilizing previous methods because of the challenges discussed above.

Since the fluorescence enhancement effect between hotspot A and B is notably different (Figure 2b), to further understand whether the fluorescence spectral modulation effect is associated with the field enhancement effect, we examined the correlation between the temporally resolved single molecule fluorescence spectrum and the fluorescence enhancement within an individual hotspot. As shown in Figure 4c (from hotspot B), the low correlation coefficient (−0.28) of these two data sets indicates that the spectral shift is not related to the electromagnetic field strength differences, which is also confirmed in the case of other hotspots. Together with the random distribution of single molecule fluorescence spectra within single hotspots (Figure 3), the above results illustrate that the single molecule fluorescence spectrum within the hotspot is not only controlled by the optical property of the resonator (i.e., the resonance frequency) but other factors (such as the polarity of the local chemical environment, the orientation of the dipole) might also affect the final pattern of the emission spectrum. These parameters should thus be carefully taken in to account in any theoretical models.

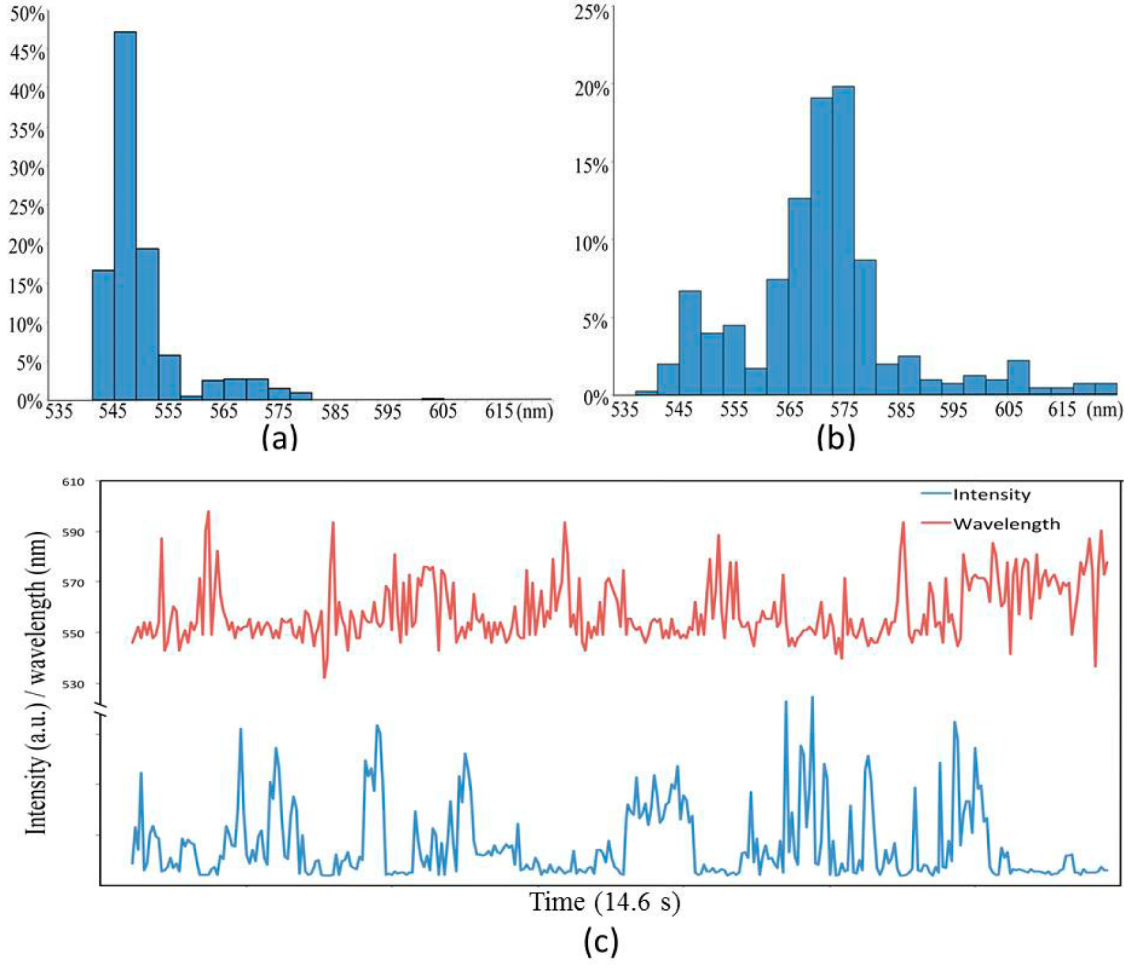

Figure 4. Histograms of single molecule fluorescence spectra within the hotspots A (a) and B (b) as shown in Figure 2b. (c) Single molecule fluorescence spectrum and intensity variations as a function of time from hotspot B.

dx.doi.org/10.1021/ac400240v | *Anal. Chem.* 2013, 85, 3789−3793

CONCLUSION

In summary, a far-field super-resolution optical imaging technique was introduced here to explore the fluorescence spectral modulation effect in nanoantennas at the single molecule level. Distinct resonant frequencies were resolved from individual hotspots for the first time. Our results show that the fluorescence spectral modulation effect inside the hotspot is a nonhomogeneous process, a feature that should be carefully considered in the future in the nanoresonator system. Furthermore, simultaneous super-resolution imaging and single-molecule spectral observation as introduced in this work was shown to be a robust platform for the extensive dynamic analyses of the optical properties of nanoresonators, for which previous methods are incapable of providing.

ASSOCIATED CONTENT

Supporting Information

Additional supporting figures as noted in the text. This material is available free of charge via the Internet at http://pubs.acs.org.

AUTHOR INFORMATION

Corresponding Author

*E-mail: lehuixiao@gmail.com (L.X.); yeung@ameslab.gov (E.S.Y.).

Author Contributions

[‖]L.W. and C.L. contributed equally.

Notes

The authors declare no competing financial interest.

ACKNOWLEDGMENTS

This work was partially supported by NSFC Grant 21205037 and the aid program for the science and technology innovation research team in higher education institutions of Hunan Province. E.S.Y. was supported by the U.S. Department of Energy, Office of Basic Energy Sciences, Division of Chemical Sciences, Geosciences, and Biosciences through the Ames Laboratory. The Ames Laboratory is operated for the U.S. Department of Energy by Iowa State University under Contract No. DEAC02-07CH11358. L.W. expresses thanks for the partial financial support from the program of China Scholarships Council. B.C. thanks the partial support from the National "863" Research Foundation (Grant 2010AA023001) and the NSFC (Grants 20927005, 21275049).

REFERENCES

(1) Kneipp, K.; Wang, Y.; Kneipp, H.; Perelman, L. T.; Itzkan, I.; Dasari, R. R.; Feld, M. S. *Phys. Rev. Lett.* **1997**, *78*, 1667−1670.
(2) Nie, S.; Emory, S. R. *Science* **1997**, *275*, 1102−1106.
(3) Shimizu, K. T.; Woo, W. K.; Fisher, B. R.; Eisler, H. J.; Bawendi, M. G. *Phys. Rev. Lett.* **2002**, *89*, 117401.
(4) Bharadwaj, P.; Novotny, L. *Opt. Express* **2007**, *15*, 14266−14274.
(5) Chen, Y.; Munechika, K.; Ginger, D. S. *Nano Lett.* **2007**, *7*, 690−696.
(6) Anger, P.; Bharadwaj, P.; Novotny, L. *Phys. Rev. Lett.* **2006**, *96*, 113002.
(7) Frimmer, M.; Chen, Y.; Koenderink, A. F. *Phys. Rev. Lett.* **2011**, *107*, 123602.
(8) Ringler, M.; Schwemer, A.; Wunderlich, M.; Nichtl, A.; Kürzinger, K.; Klar, T. A.; Feldmann, J. *Phys. Rev. Lett.* **2008**, *100*, 203002.
(9) Imura, K.; Nagahara, T.; Okamoto, H. *J. Chem. Phys.* **2005**, *122*, 154701.
(10) Ghenuche, P.; Cherukulappurath, S.; Taminiau, T. H.; Hulst, N. F. v.; Quidant, R. *Phys. Rev. Lett.* **2008**, *101*, 116805.
(11) Sun, Y.; Yin, Y.; Mayers, B.; Herricks, T.; Xia, Y. *Chem. Mater.* **2002**, *14*, 4736−4745.
(12) Yildiz, A.; Forkey, J. N.; McKinney, S. A.; Ha, T.; Goldman, Y. E.; Selvin, P. R. *Science* **2003**, *300*, 2061−2065.
(13) Thompson, R. E.; Larson, D. R.; Webb, W. W. *Biophys. J.* **2002**, *82*, 2775−2783.
(14) Lee, S. J.; Baik, J. M.; Moskovits, M. *Nano Lett.* **2008**, *8*, 3244.
(15) Rust, M. J.; Bates, M.; Zhuang, X. *Nat. Methods* **2006**, *3*, 793−796.
(16) Betzig, E.; Patterson, G. H.; Sougrat, R.; Lindwasser, W.; Olenych, S.; Bonifacino, J. S.; Davidson, M. W.; Lippincott-Schwartz, J.; Hess, H. F. *Science* **2006**, *313*, 1642−1645.
(17) Wu, D.; Liu, Z.; Sun, C.; Zhang, X. *Nano Lett.* **2008**, *8*, 1159−1162.
(18) Sharonov, A.; Hochstrasser, R. M. *Proc. Natl. Acad. Sci. U.S.A.* **2006**, *103*, 18911−18916.
(19) Cang, H.; Labno, A.; Lu, C.; Yin, X.; Liu, M.; Gladden, C.; Liu, Y.; Zhang, X. *Nature* **2011**, *469*, 385−388.
(20) Willets, K. A.; Stranahan, S. M.; Weber, M. L. *J. Phys. Chem. Lett* **2012**, *3*, 1286−1294.
(21) Stranahan, S. M.; Willets, K. A. *Nano Lett.* **2010**, *10*, 3777−3784.
(22) Xiao, L.; He, Y.; Yeung, E. S. *J. Phys. Chem. C* **2009**, *113*, 5991−5997.